Cellulose (2022) 29:4083–4095
https://doi.org/10.1007/s10570-022-04524-7

ORIGINAL RESEARCH

Highly sensitive and selective fluorescent sensor for Ag^+ detection using β-cyclodextrin/chitosan polymer-coated S QDs based on an aggregation-induced quenching mechanism

Shan Wang · Huan Wang · Jianshe Yue · Yi Lu · Tian Jia · Jie Chen

Received: 12 January 2021 / Accepted: 1 October 2021 / Published online: 2 April 2022

Abstract A novel sensor for the sensitive and selective detection of Ag^+ based on poly(β-cyclodextrin/chitosan (CTSCD) with H-bonded sulphur quantum dots (QDs) was synthesized by self-assembly. S QDs on the CTSCD chain can coordinate with transition metal ions due to surface electronegativity. The distance between S QDs and Ag^+ can form bridge S–Ag^+–S bonds with Ag^+. These are associated with noncovalent bonds to form Ag^+-based S QD/CTSCD nanocomposite aggregates, leading to fluorescence aggregation-induced quenching. By utilizing S QD/CTSCD as a sensor to detect Ag^+, a good linear relationship in the range of 1.0×10^{-5} to 5.5×10^{-5} mol/L ($R^2=0.9992$) was obtained. Moreover, the S QD/CTSCD nanocomposite was successfully utilized to monitor Ag^+ in river water with satisfactory performance. This work offers a new paradigm for the design of novel composite sensors with good sensitivity and selectivity.

Keywords S QDs · CTSCD nanocomposites · Silver ions · Fluorescent · Sensor

S. Wang (✉) · H. Wang · J. Yue · Y. Lu · T. Jia · J. Chen
School of Chemistry and Chemical Engineering, Xianyang Normal University, Xianyang 712000, People's Republic of China
e-mail: shanwang2005@163.com

Introduction

Silver is widely used in the electronics, photosensing, and electroplating industries (Singha et al. 2015; Liu et al., 2008; Zhou et al. 2021). The overuse of silver has triggered a serious environmental crisis (Velmurugan et al. 2014). Ag^+ is one of the most toxic metal ions for aquatic organisms because the accumulation of Ag^+ can inactivate sulfhydryl enzymes and combine with imidazole carboxyl groups and amines in various metabolites. Thus, the detection and analysis of Ag^+ is an important topic for health, epidemic prevention, and environmental monitoring. There are many ways to detect heavy metal ions, such as stripping voltammetry Xiao et al. 2010, atomic absorption spectrometry Luidmila et al. 2017, and inductively coupled plasma mass spectrometry Spokoyny et al. 2009. All of these methods are nonportable, expensive, and time-consuming (Lotfia et al. 2017). Fluorescence analysis, a highly sensitive and selective determination method, has developed rapidly in recent years (Wang et al. 2019). This method can not only be used to overcome the above shortcomings but also solve serious drawbacks, such as low sensitivity, hydrophobicity, low selectivity, and toxicity (Vaishnav and Mukherjee 2019; Jiang et al. 2018; Wang et al., 2019). Moreover, Ag^+ is an effective fluorescence quenching agent for heavy metal ions. If appropriate substances are selected, fluorescence quenching for detecting trace Ag^+ can be established.

As long as appropriate substances are selected, fluorescence quenching for detecting trace silver ions has been established in recent years (Djerahov et al. 2016). A few sensors, including sulphur atoms, have been reported for silver ion determination in recent years (Prasannan and Imae 2013; Park et al. 2015). However, many of these sensors have poor biocompatibility and poor water solubility, which hinders their application in water and biological environments. Therefore, the development of biocompatible and water-soluble fluorescent sensors for silver ions is one of the fields that scientists focus on. To date, a wide variety of fluorescent sensors have been developed, including metal nanoparticles, QDs and dye molecules, to solve the disadvantages of low sensitivity, low selectivity, insolubility toxicity and so on (Jiang et al. 2015). S QDs have attracted much attention because of their unique stability, low cytotoxicity and high biocompatibility. To date, S QDs as a new nanomaterial have played a vital role in many applications. It was found that there almost no fluorescent sensors are available to detect silver ions by S QDs (Lv et al. 2014). Therefore, it is necessary to develop high-sensitivity, green, portable, and low-cost S QD fluorescence sensors to detect silver ions.

Several coordination mechanism-based sensors for detecting ions have been exploited (Gao et al. 2015; Wang et al. 2007). Polymers have a tailorable and diversified structure and provide a new possibility for use as biosensors (Tabaraki and Nateghi 2016; Bian et al. 2016; Vaishnav and Mukherjee 2019; Jiang et al. 2018). However, most of these coordination polymers are macroscopic solid-state substances, which show very limited solution-based behaviour. These properties remarkably limit their application in biosensors.

We proposed a novel method to detect Ag^+ with high sensitivity and excellent selectivity. Chitosan (CTS) and β-cyclodextrin (β-CD) was used to form a CTSCD polymer by formaldehyde, and the replicates of the experiment exceeded 85% (Binti et al. 2020). The cross-linked polymer solved the problems of poor biocompatibility and poor water solubility, and the reaction can be represented by a simple structure diagram as follows: S QDs combine with the amino group of CTSCD by an electrostatic effect to form S QDs/CTSCD nanocomposites. S QD/CTSCD nanocomposites rapidly aggregate in the presence of Ag^+ because of their attraction to the surroundings of the S QD/CTSCD nanocomposites through electrostatic interactions. S–Ag^+–S bonds are formed with S QD/CTSCD nanocomposites, leading to remarkable particle aggregation, and the fluorescence mechanism should involve aggregation-induced quenching (AIQ). A possible mechanism is shown in Fig. 1. To the best of our knowledge, this is the first study employing a

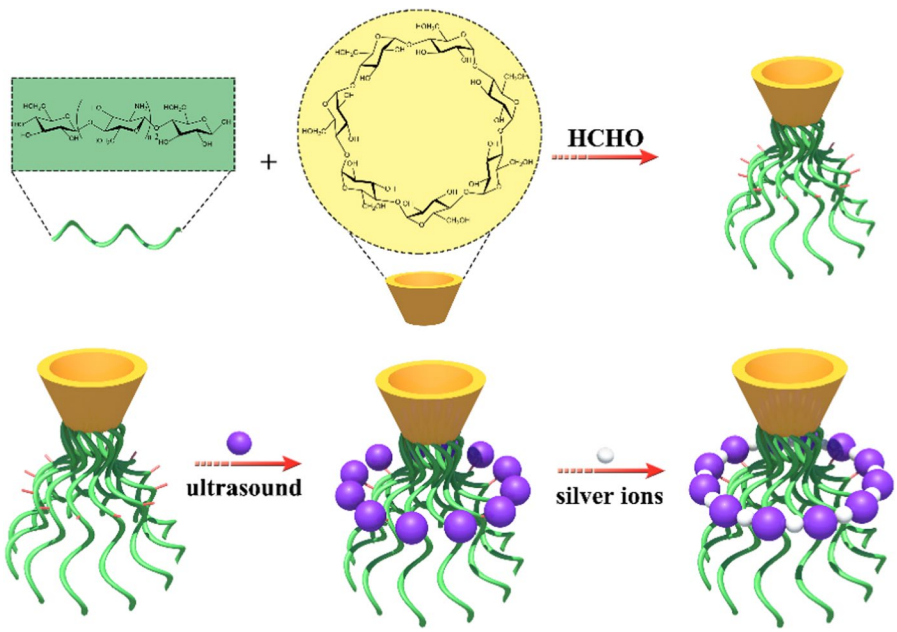

Fig. 1 Possible mechanism for the S QD/CTSCD nanocomposite sensor operation

facile self-assembly method to obtain S QD/CTSCD nanocomposites for Ag^+ by an AIQ mechanism.

Experimental

Reagents and instruments

All chemical reagents were purchased from Aldrich and used without further purification. Fluorescence was recorded using a Fluoromax-F7000 with a 10 nm slit, and UV–Vis spectra were obtained using Shimadzu UV-24500 equipment. X-ray photoelectron spectroscopy (XPS) was carried out by using an axisultra DLD electron spectrometer from Shimadzu. Fourier-transform infrared (FTIR) spectra were obtained by using a Nicolet Magna 550 spectrometer. The morphology of the S QDs was observed by a JEOL JEM 2100 transmission electron microscope.

Preparation of CTSCD composites

Exactly 3.000 g CTS was completely dissolved in 300.0 mL (0.1000 mol L^{-1}) hydrochloric acid, and 15.00 g β-CD was dissolved in 600.0 mL distilled water. The above solutions were mixed in a 1000.0 mL beaker, heated to 333.0 K, and then slowly added to 14.40 mL (25.00%) formaldehyde. The temperature of the solution was increased to 363.0 K, and the reaction was carried out under stirring for 80.00 min. After the reaction was completed, NaOH was added dropwise into the solution until pH = 11.00, and a yellow precipitate was produced. The same temperature was maintained, and the reaction was continued for 45.00 min, filtered, and then washed with acetone and ethanol to neutral pH. The product was dried at 318.0 K until a constant weight was achieved (Binti et al. 2020). CTSCD composites (the scheme is shown in Fig. 2) showed a red–brown colour (the replicate rate of the experiment exceeded 85%).

S QD-functionalized CTSCD composites

Exactly 0.04 g CTSCD was dissolved in 6.00 mL anhydrous ethanol. S QDs (1.4852 mL (3.00 mg/mL)) were added into the solution. The mixture was reacted for approximately 30 min by ultrasound, and S QD/CTSCD nanocomposites were obtained.

Fluorescence properties of S QD/CTSCD nanocomposites

The fluorescence sensing properties of S QD/CTSCD nanocomposites were determined by adding a fixed amount of S QD/CTSCD nanocomposites (500 μL) to samples containing varying Ag^+ concentrations, and the corresponding fluorescence spectra were recorded. The Ag^+ content in the sample was determined as follows: Different concentrations of Ag^+ were mixed with 500 μL S QD/CTSCD nanocomposites and 2.5 mL ultrapure water. After 5 min, the solution was subjected to luminous measurement at $\lambda_{ex} = 295$ nm. The λ_{ex} for the S QD/CTSCD nanocomposites was 295 nm in all tests, and the emission was monitored from 320 to 580 nm. The width of the excitation and emission slits was 5 nm.

The selectivity for Ag^+ detection was investigated by preparing the same samples following the above method. Fe^{3+}, Ca^{2+}, Pb^{2+}, Na^+, Cr^{3+}, Bi^{3+}, Zn^{2+}, Mg^{2+}, Ba^{2+}, Cd^{2+}, Ag^+, Sr^{2+}, Hg^{2+}, Ni^{2+}, Ag^+, and other solutions were added to each sample until the same concentration (10 μM) was reached. All mixtures were incubated at room temperature for 20 min.

Application to actual water samples

The practicability of the sensors was evaluated by detecting samples obtained from Xianyang Lake, Gudu River, and tap water at different places in Xianyang. Impurities were removed by filtration and centrifugation, and the Ag^+ ions in the samples were detected by using the standard method. The detection procedure was the same as the above procedure.

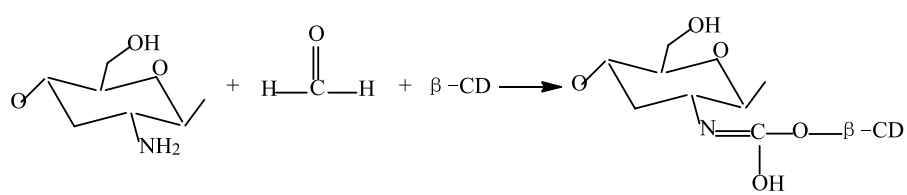

Fig. 2 The reaction scheme used to prepare CTSCD composites

Results and discussion

FTIR spectroscopy and DSC for S QD/CTSCD nanocomposites

Figure 3a shows the infrared spectra for the S QD, CTS/β-CD, and S QDs/CTSCD nanocomposites. The peak at 1640 cm^{-1} is a typical characteristic of S QDs (Wang et al. 2019), and the peak at 896 cm^{-1} is attributed to the β-(1, 4)-glycosidic bonds of CTS. The peak at 1042 cm^{-1} indicates the presence of the α-(1, 4)-glycosidic bond of β-CD. The peak at 1640 cm^{-1} corresponds to S QDs, indicating that S is successfully introduced into the CTSCD composites. The peaks at 1560–1640 and 2100 cm^{-1} are mostly attributed to amino ($–NH_2$), alicyclic amine I (C=O), and cyclic amine II (N–H) groups. The absorption peak for the S QDs/CTSCD nanocomposite was reduced due to the reaction with the amino group. The absorption peak for the composite at 3440 cm^{-1} was enhanced because of the tensile vibration peak for –OH.

The DSC results for the CTS/β-CD and S QD/CTSCD nanocomposites are shown in Figs. 3b. The curve shows an evident endothermic peak at 97.25 °C, which is attributed to the crystalline water that evaporates from CTSCD. The melting peak for CTS occurs at approximately 225 °C due to the internal H bond, whereas the melting peak for CTSCD occurs at approximately 228 °C, indicating a greater stability compared to the CTS monomer (Djerahov et al. 2016; Teng et al. 2020a, b; Rao et al. 2020; Li et al. 2020; Li et al. 2020). From the curve for the S QDs/CTSCD nanocomposites shown in Fig. 3b, an evident endothermic peak is found at 100.30 °C. The results show that the thermal stability of CTSCD is improved because S QDs are successfully introduced into the CTSCD composites. The exothermic peak at 259.48 °C indicates the degradation peak for the S QD/CTSCD nanocomposite chain, which is due to the weakening of hydrogen bond interactions and the destruction of structure regulation by S QDs. The two lines in Fig. 3b show that S QDs improve the thermal stability of S QD/CTSCD nanocomposites by increasing the degradation temperature of the chain skeleton.

The optical properties and TEM for S QD/CTSCD nanocomposites

The optical properties of the S QD/CTSCD were studied by UV absorption and fluorescence spectra at room temperature. Figure 4a shows a 298 nm peak in the UV absorption spectrum. The ultraviolet absorption for S QDs, which is modified by the CTSCD polymer, is stronger than that of S QDs. Therefore, as shown in Fig. 4a, the S QD/CTSCD nanocomposite solution is light yellow (a) in sunlight but bright blue when irradiated with 365 nm UV light (b), indicating the blue fluorescence properties of the S QD/CTSCD nanocomposites. When excited at 295 nm, the fluorescence spectrum shows an excellent emission peak at approximately 411 nm, which is shown in Fig. 4b.

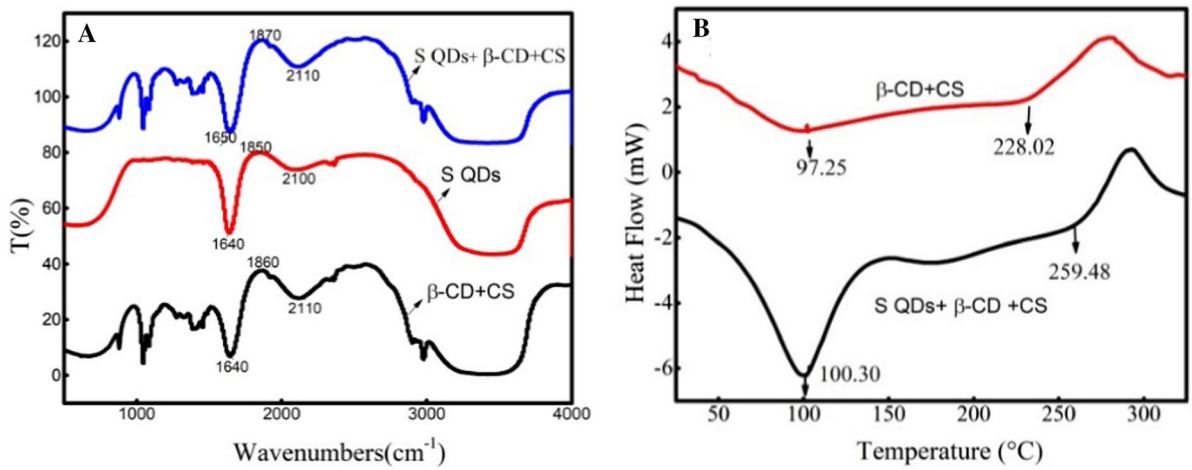

Fig. 3 FTIR (**a**) and DSC (**b**) spectra for the S QD/CTSCD nanocomposites

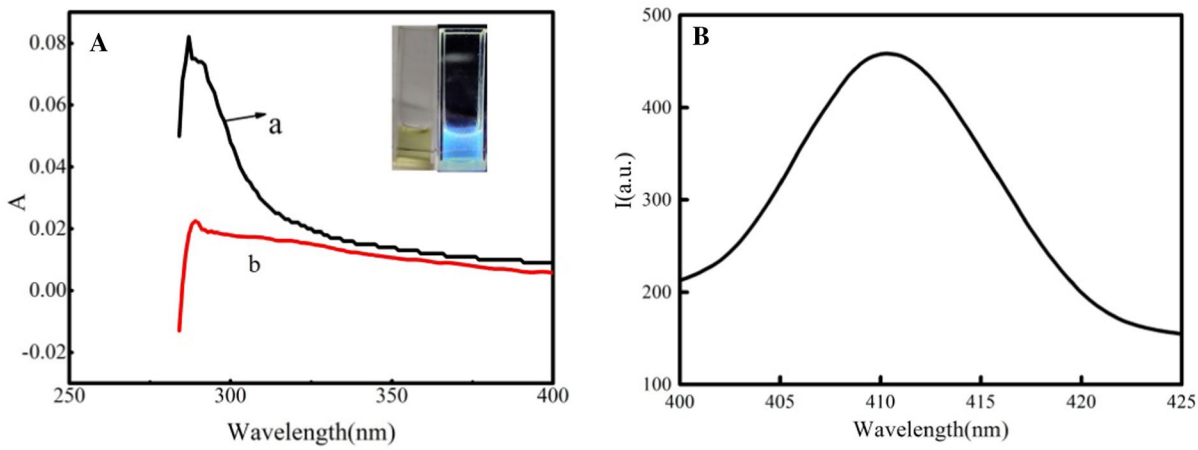

Fig. 4 UV/Vis spectra (**a**) and fluorescence emission (**b**) for the S QD/CTSCD nanocomposites

TEM micrographs (Fig. 5a) show a good dispersion of S QDs in water. Particles mostly show a regular spherical shape with a size of approximately 2–3 nm. A typical amorphous structure is observed with no visible lattice. The results show that S QDs have excellent nanoparticle properties. The atomic force microscopy (AFM) image shows the shape and height of the S QDs. The average height is 0.8 nm (Fig. 5b). The TEM image shows the good dispersion

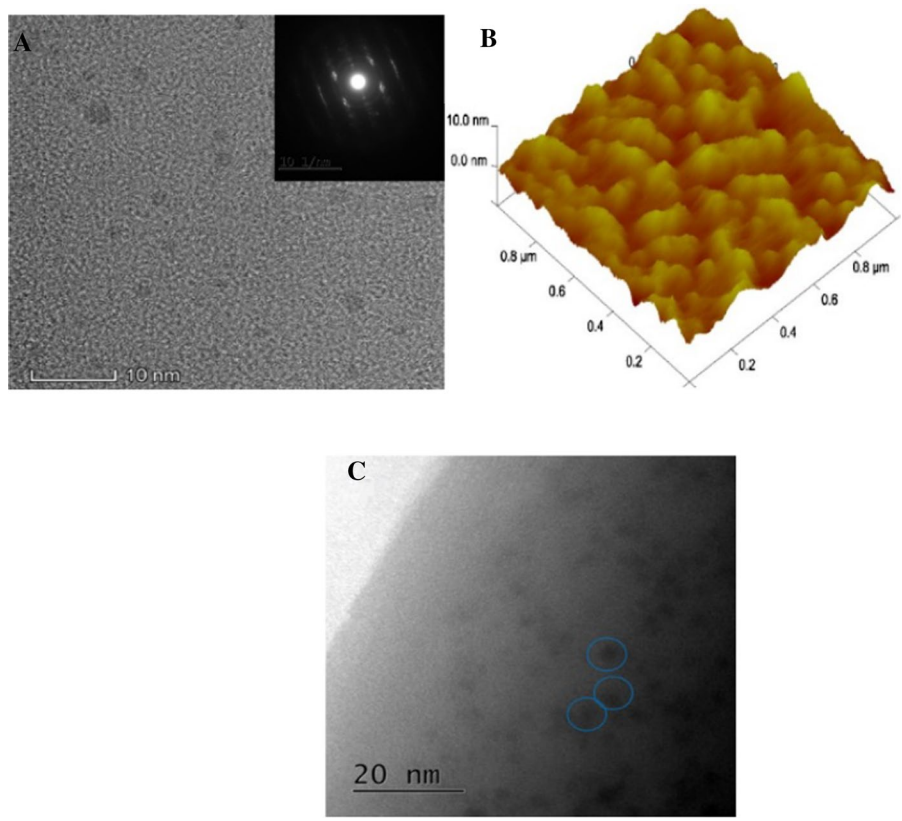

Fig. 5 **a** TEM image of S QDs with diameters of approximately 2–3 nm; **b** AFM representation of S QDs; and **c** TEM for the S QD/CTSCD nanocomposites

of S QD/CTSCD (Fig. 5b, c) with a relatively uniform size distribution.

XPS for S QD/CTSCD nanocomposites

The composition, surface group, and structure of the S QD/CTSCD were studied by XPS. The nanocomposites show four peaks at 165.9 eV, 284.30 eV, 398.8 eV, and 532.04 eV (Fig. 6a) representing S2p, C 1 s, N 1 s, and O 1 s in the XPS spectra, respectively. The XPS results show that the nanocomposites are primarily comprised of S, C, O, and N. The C 1 s spectrum (Fig. 6b) shows two peaks at 282.73 eV and 285.9 eV, which should be attributed to C–C and C–OH, respectively. Three peaks are found at 165.75 eV, 166.25 eV, and 165.5 eV in the S2p spectra (Fig. 6c), which are attributed to the SO_2^- ($2p^{1/2}$), SO_3^- ($2p^{2/3}$), and SO_3^- ($2p^{1/2}$) bands, respectively. The two peaks at 395.9 eV and 397.1 eV in the N 1 s spectrum (Fig. 6d) are attributed to the C–N–C and C–N groups, respectively. The O 1 s spectrum (Fig. 6e) shows two peaks at 532.7 eV and 531.9 eV, which are due to the C–OH/C–O–C and C = O bands, respectively (Park et al. 2015; Teng et al. 2018; Wu et al. 2020). The results indicate that S QDs are already successfully introduced into CTSCD composites.

The effect of pH on the fluorescence properties

Figure 7 shows the effect of pH on the fluorescence properties of the S QD/CTSCD solution. In the experiments, 0.1 M HCl and NaOH were added to the solution to obtain the desired pH (4–10). In a strong acid environment (pH ≤ 4), the amino groups on chitosan protonate (Gao et al. 2014; Yang et al. 2020) and destroy the weak self-assembly between the CTSCD polymer and S QDs. S QDs can detach from the polymer chain, and the fluorescence intensity can increase significantly (pH = 4). With increased pH, the fluorescence intensity decreases by approximately 7%. This negligible change might be the result of a small change in the quantum confinement due to functionalization of the S QD/CTSCD. S QD/CTSCD samples did not show a change in their maximum fluorescence emission value (λ_{em}) or shape. Under the experimental conditions, the S QD/CTSCD samples were monodispersed, and the fluorescence emission was stable (Dager et al. 2019).

The selectivity of the sensor

Selectivity is an important parameter for assessing fluorescence properties. The effects of metal ions, such as Fe^{3+}, Ca^{2+}, Pb^{2+}, Na^+, Cr^{3+}, Bi^{3+}, Zn^{2+}, Mg^{2+}, Ba^{2+}, Cd^{2+}, Ag^+, Sr^{2+}, Hg^{2+}, and Ni^{2+}, at a fluorescence concentration of 1.0×10^{-5} mol/L were examined. As shown in Fig. 8a, the fluorescence intensity from S QD/CTSCD nanocomposites in the presence of Ag^+ is quenched to a remarkable extent, whereas that in the presence of other metal ions (e.g., alkali, alkali soil, and transition metal ions) at 1.0×10^{-5} mol/L shows negligible changes or remains unchanged. Thus, a sensor based on S QD/CTSCD shows good selectivity towards Ag^+.

The sensing properties of the S QD/CTSCD nanocomposite for silver ions

Under optimum conditions, the sensitivity of the S QD/CTSCD nanocomposite towards Ag^+ was investigated. In a typical operation, the S QD/CTSCD solution (0.01 mg mL^{-1}) was dispersed in water and mixed with varying amounts of Ag^+. After the samples were incubated at room temperature for 10 min, the fluorescence emission spectra were recorded and analysed in triplicate. The fluorescence intensity was calibrated by changing the Ag^+ concentration.

Figure 8b shows that the fluorescence peak for the S QD/CTSCD nanocomposites gradually decreases with increasing Ag + concentration because of the S–Ag^+–S bonds formed between Ag^+ and the S QD/CTSCD nanocomposites. Based on this phenomena, a favourable linear correlation exists ($R^2 = 0.9992$) between I and Ag^+ at concentrations ranging from 1×10^{-5} to 5.5×10^{-5} mol/L (Fig. 8c), and the detection limit for Ag^+ based on the 3δ/slope was determined to be approximately 85 nM. The effectiveness of Ag^+ fluorescence detection with S QDs/CTSCD as a fluorescence probe was verified, which provides a platform for Ag^+ detection. The selectivity of S QD/CTSCD nanocomposites for Ag^+ might be due to the synergistic effect of S and O functional groups on S QD/CTSCD nanocomposites (Nam et al. 2017). F_0 is [C] = 0, where F is the fluorescence intensity before and after adding Ag^+, K_{SV} is the quenching effect coefficient of the sensing material, and [C] is the molar concentration of the analyte.

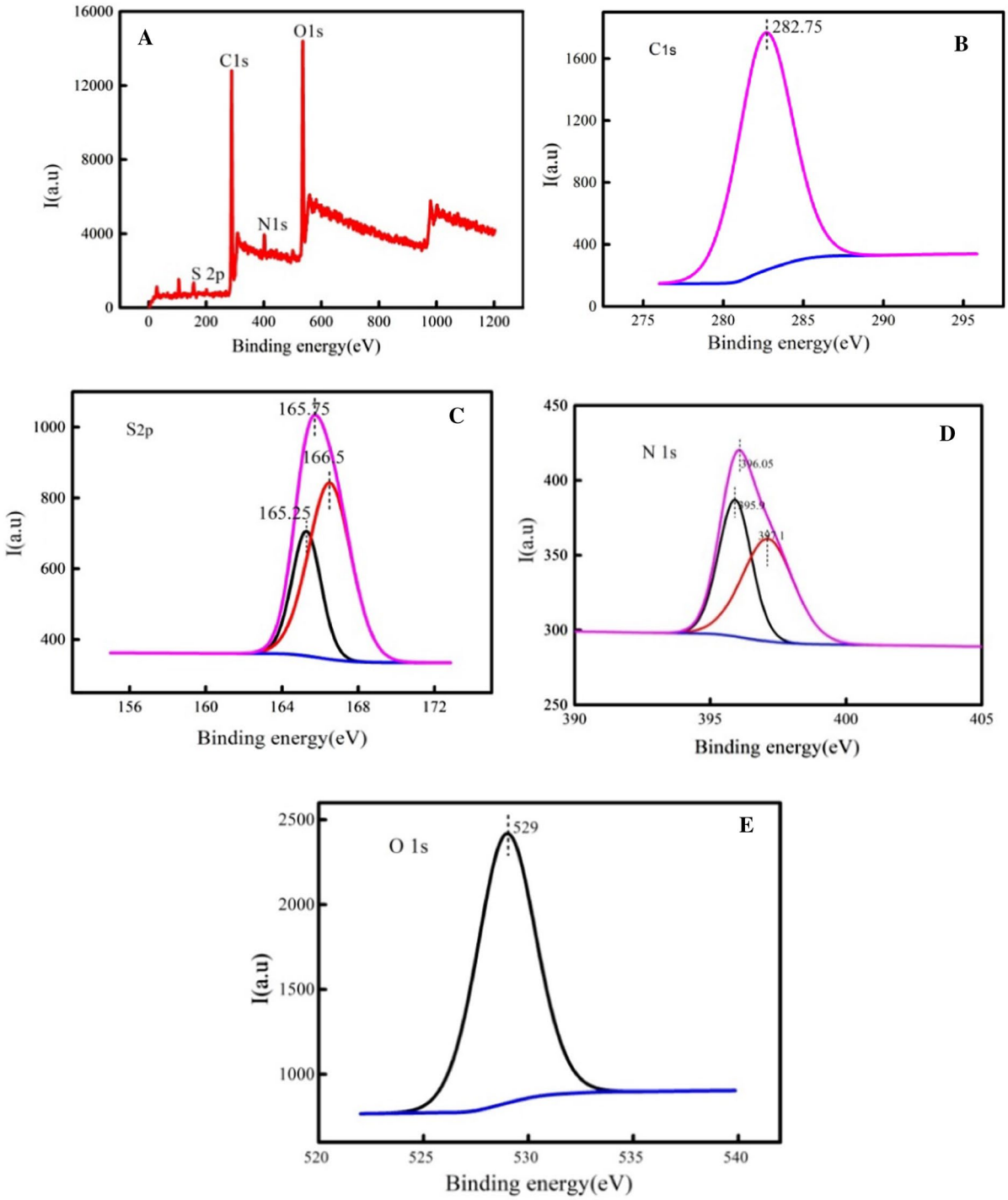

Fig. 6 XPS for the S QD/CTSCD nanocomposites

When Sb is a blank signal standard deviation, the Ag^+ (C) concentration is linear with a decreased Ag^+ (C) concentration in the range of 1×10^{-5} to 5.5×10^{-5} mol/L ($I_0/I=1+0.0029C$ [$R^2=0.9969$]).

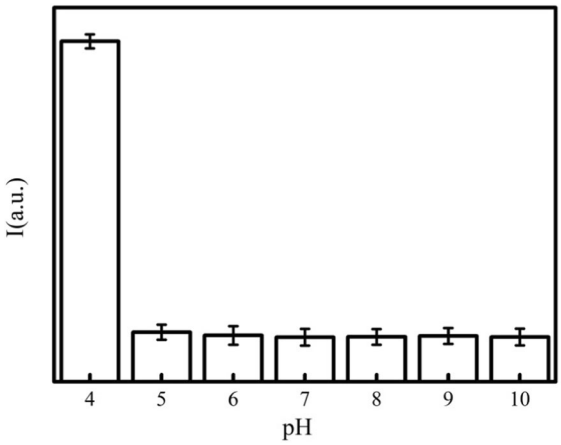

Fig. 7 The effect of pH on the fluorescence properties of S QD/CTSCD nanocomposites

The concentration of silver ions ranges from 1.0×10^{-5}–5.5×10^{-5} mol/L (Fig. 8d). The results show that the S QD/CTSCD nanocomposite is a more sensitive fluorescence sensor of silver ions compared to other sensors (Lu et al. 2014; Jiang et al. 2015). The sensitivity of the Ag^+ sensor is higher than that of other methods reported in the literature (Lv et al. 2014; Gao et al. 2015; Wang et al. 2007). As shown in Table 1, the detection limit and the analytical concentration range for different technologies (e.g., electrochemical, high-performance liquid chromatography, and other methods) are much lower than that for the proposed sensor. Solid-phase microextraction, which is used as a detector in liquid chromatography-tandem mass spectrometry, is comparable with the proposed sensor. However, as reported in the literature, these processes are expensive, time-consuming, and inconvenient. Our sensor shows satisfactory properties in terms of analysis time, sensitivity, cost, and operation (on-site analysis) and can be used to detect Ag^+ directly in actual samples. The quenching effect can be rationalized by the Stern–Volmer equation: $I_0/I = 1 + 0.0029C$ ($R^2 = 0.9966$).

3.7 Sensor mechanism

A simple method for synthesizing fluorescent S QD/CTSCD nanocomposites that possess fluorescence detection was presented. The functionalization of S QDs on the CTSCD structure is determined by the ability of the functional group. Ag^+ serves as a coordinating centre that directly reacts with S QDs on the CTSCD chain. The hydration radius of Ag^+ can exactly match the distance on the S QD-functionalized CTSCD structure. S QD-functionalized CTSCD supramolecular structures are promising because their structure contains potential coordination centres comprising metal cations. S QDs in the polymer structure form S–Ag^+–S bonds with Ag^+ ions, which combine with colloidal particles with noncovalent bonds and form a dendritic fractal structure of aggregates based on Ag^+. The fluorescence mechanism should be aggregation-induced quenching (AIQ).

The effect of the metal ions

The recognition property of the sensor against various metal ions was explored by using the fluorescence response to Ag^+. The effect of some coexisting cations on the detection of Ag^+ is shown in Fig. 9. Most coexisting metal ions do not interfere with the binding of Ag^+ to the S QD/CTSCD nanocomposites except for Ni^{2+} ions, which have a weak effect on detection. Therefore, the selective binding of Ag^+ can be carried out in the presence of the most competitive and coexisting metal ions.

Detecting silver ions in environmental samples

The sensing properties of S QD/CTSCD nanocomposites were analysed in river water (Xianyang Lake, Gudu River, and Nanhu Lake in Xianyang, China). Similar to the results obtained for distilled water, the fluorescence intensity of the S QD/CTSCD nanocomposites in river water drops after adding Ag^+. Although there various substances are present in river water that can interfere with the detection of Ag^+, the results show that the recovery of Ag^+ in the sample is 98.44–110.76% (Table 2). The measured values show that the designed sensor is reliable and practical in different environmental water samples. Therefore, the S QD/CTSCD nanocomposites exhibit fluorescence properties that are sensitive and selective to Ag^+.

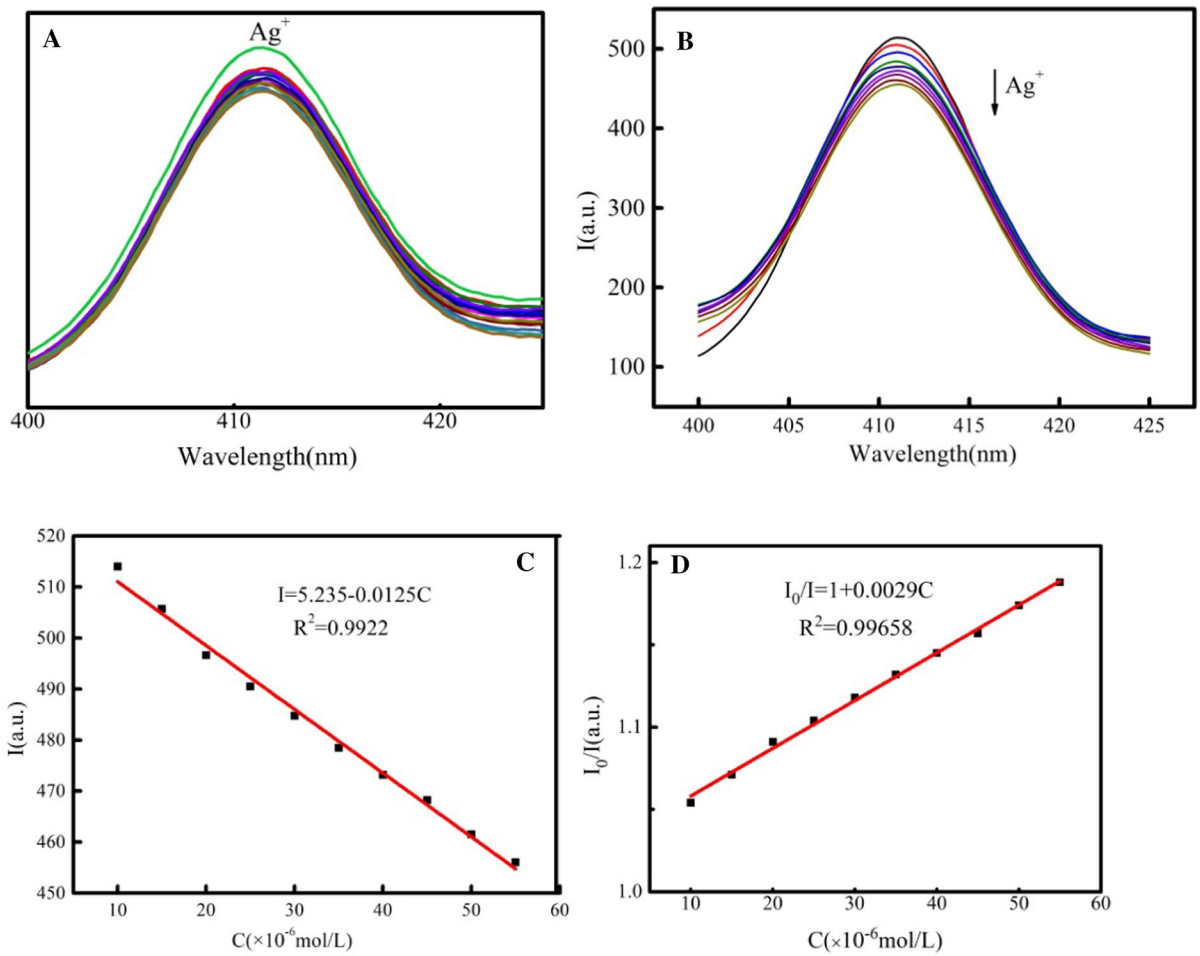

Fig. 8 The sensing properties of S QD/CTSCD nanocomposites (A, Selectivity; B, Sensing properties (silver ion concentration from 1×10^{-5} mol/L to 5.5×10^{-5} mol/L);C, Linear properties; D, S-V equation;C Ag^+: 1,1×10^{-5} mol/L; 2,1.5×10^{-5} mol/L; 3, 2×10^{-5} mol/L; 4, 2.5×10^{-5} mol/L; 5, 3×10^{-5} mol/L; 6, 3.5×10^{-5} mol/L; 7, 4×10^{-5} mol/L; 8, 4.5×10^{-5} mol/L; 9, 5×10^{-5} mol/L; 10, 5.5×10^{-5} mol/L)

Conclusion

We demonstrated a facile strategy to synthesize S QD/CTSCD nanocomposites via self-assembly. The fluorescence from S QD/CTSCD nanocomposites can be sensitively and selectively quenched by Ag^+ based on an aggregation-induced quenching mechanism. The advantages of these nanocomposites are summarized in the following aspects: (1) S-QDs are successfully linked to the CTSCD polymer chain through a simple and convenient ultrasonic reaction. S QD/CTSCD exhibit excellent fluorescence behaviour; (2) S QD/CTSCD show a good selective and sensitive response to Ag^+; (3) A simple and direct method to detect Ag^+ was realized with a fast response, wide linear range, and low detection limit; (4) Actual samples from the environment were analysed, and the results show that the error rate detection for Ag^+ is less than 11%. The novel sensor is easily synthesized by a simple process and has broad application prospects in the field of sensing.

Table 1 Comparisonof various fluorescence sensors used to detect silver ions

Fluorescent probe	DL (μM)	Linear range (μM)	Ref
C QDs	0.075	0.2–50	Li et al. (2019)
Q Cy(NIR) fluorescent	0.03	–	Zhang et al. (2019)
Pyrene	0.077	0–90	Kim et al. (2020)
NBOS	4.24	0.08–10.66	Li et al. (2020)
PPN(nopinone)	0.86	0.2–40	Jiang et al. (2020)
S-doped GQDs	0.03	0.1–130	Tabaraki et al. (2016)
S QDs/CTSCD	0.085	0.01–0.055	Present work

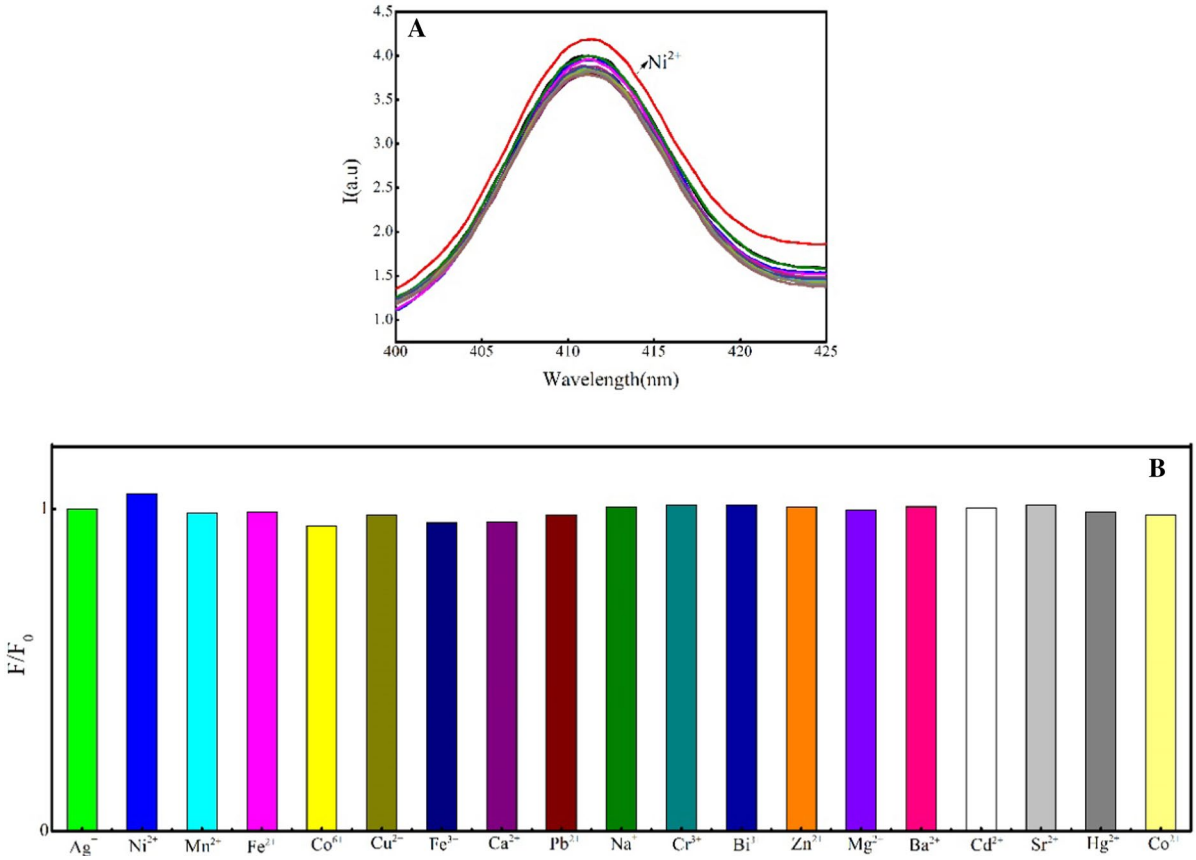

Fig. 9 Metal ion interference during Ag + sensing by S QD/CTSCD nanocomposites (**a**: Fluorescent spectrogram; **b**: Histogram)

Table 2 A comparison of the different samples used to analyse the detection of silver ions

Sample	Added silver ions (μM)	Detection silver ions (μM)	Recovery percent (%)
Distilled water	0.005	0.00505	101
Tap-water	0.005	0.00495	99
Xianyang lake	0.005	0.0055	110
Nanhu	0.005	0.4922	98.44
Gudu canal	0.005	0.0055	110.76

Acknowledgements This work was supported by the National Natural Science Foundation of China (No. 21703189) and the Xianyang Science and Technology Bureau Project (2019K02–27). Xianyang Normal University project (2019K0237).

Funding The authors have not disclosed any funding.

Data availability The data that support the findings of this study are available from the corresponding author upon reasonable request.

Declarations

Conflict of interest The authors declare that they have no known competing financial interests or personal relationships that could have appeared to influence the work reported in this paper. The experiment complies with ethical approval statements and ethical standards.

References

Barriada JL, Tappin AD, Evans EH, Achterberg EP (2007) Dissolved silver measurements in seawater. TrAC Trends Anal Chemi 26:809–817. https://doi.org/10.1016/j.trac.2007.06.004

Bian S, Shen C, Qian Y, Liu J, Dong X (2016) Facile synthesis of sulfur -doped graphene quantum dots as fluorescent sensing probes for Ag^+ ions detection. Sens Actuators, B Chem 242:231–237. https://doi.org/10.1016/j.snb.2016.11.044

Binti S, Harpreet S, Madhu K et al (2020) Immobilization of keratinase on chitosan grafted β- cyclodextrin for the improvement of the enzyme properties and application of free keratinase in the textile industry. Int J Biol Macromol. https://doi.org/10.1016/j.ijbiomac.2020.10.009

Chamsaz M, Arbab-Zavar MH, Akhondzadeh J (2008) Triple-phase single-drop microextraction of silver and its determination using graphite-furnace atomic- absorption spectrometry. Anal Sci Int J Jpn Society Anal Chem 24:799–801. https://doi.org/10.2116/analsci.24.799

Dager A, Uchida T, Maekawa T, Tachibana M (2019) Synthesis and characterization of mono-disperse carbon quantum dots from fennel seeds: photoluminescence analysis using machine learning. Sci Rep. https://doi.org/10.1038/s41598-019-50397-5

Ding C, Zhu A, Tian Y (2013) Functional surface engineering of C-Dots for fluorescent biosensing and in vivo bioimaging. Acc Chem Res 47:20. https://doi.org/10.1021/ar400023s

Djerahov L, Vasileva P, Karadjova I, Kurakalva RM, Aradhi KK (2016) Chitosan film loaded with silver nanoparticles- sorbent for solid phase extraction of Al(III), Cd(II), Cu(II), Co(II), Fe(III), Ni(II), Pb(II) and Zn(II). Carbohyd Polym. https://doi.org/10.1016/j.carbpol.2016.03.080

Fu L, Wang A, Xie K, Zhu J, Chen F, Wang H, Zhang H, Su W, Wang Z, Zhou C (2020) Electrochemical detection of silver ions by using sulfur quantum dots modified gold electrode. Sens Actuators 304:127391–127397. https://doi.org/10.1016/j.snb.2019.127390

Gao C, Liu T, Dang Y et al (2014) pH /redox responsive core cross-linked nanoparticles from thiolated carboxymethyl chitosan for in vitro release study of methotrexate. Carbohyd Polym 111:964–970. https://doi.org/10.1016/j.carbpol.2014.05.012

Gao X, Lu Y, Zhang R, He S, Ju J, Liu M, Li L, Chen W (2015) One-pot synthesis of carbon nanodots for fluorescence turn-on detection of Ag^+ based on the Ag^+-induced enhancement of fluorescence. J Mater Chem C 3:2302–2309. https://doi.org/10.1016/j.carbpol.2014.05.012

Hwang KS, Park KY, Kim DB, Chang SK (2017) Fluorescence sensing of Ag^+ ions by desulfurization of an acetylthiourea derivative of 2-(2-hydroxyphenyl) benzothiazole. Dyes Pigm. https://doi.org/10.1016/j.dyepig.2017.08.041

Jaiswal A, Ghosh SS, Chattopadhyay A (2011) One step synthesis of C-dots by microwave mediated caramelization of poly (ethylene glycol). Chem Commun Ications 48:407–409. https://doi.org/10.1039/c1cc15988g

Jiang Y, Kong W, Shen Y, Wang B (2015) Two fluorescence turn-on chemosensors based on pyrrolo[2,1-a]isoquinoline for detection of Ag^+ in aqueous solution. Tetrahedron 71:5584–5588. https://doi.org/10.1016/j.tet.2015.06.055

Jiang X, Yusuke I, Chong W, Shofiur R, Paris G, Xi Z, Mark E, Carl R, Simon T, Takehiko Y (2018) A hexahomotrioxacalix[3] arene-based ditopic receptor for alkylammonium ions controlled by Ag^+ ions. Molecules 23:467. https://doi.org/10.3390/molecules23020467

Jiang Q, Wang Z, Li M, Song J, Yang Y, Xu X, Xu H, Wang S (2020) A nopinone basedmultifunctional probe for colorimetric detection of Cu^{2+} and ratiometric detection of Ag^+. J Photochem Photobiol 19(1):49–55. https://doi.org/10.1039/c9pp00297a

Kim S, Lee H, Ju BC, Kim C (2020) A pyrene-mercapto-based probe for detecting Ag^+ by fluorescence turn-on. Inorg Chem Commun 118:108044. https://doi.org/10.1016/j.inoche.2020.108044

Li C, Zhang X, Zhang W, Qin X, Zhu C (2019) Carbon quantum dots derived from pure solvent tetrahydrofuran as a fluorescent probe to detect pH and silver ion. J Photochem Photobiol, A 382:111981. https://doi.org/10.1016/j.jphotochem.2019.111981

Li R, Fan H, Shen L, Rao L, Tang J, Hu S, Lin H (2020) Inkjet printing assisted fabrication of polyphenol-based coating membranes for oil/water separation. Chemosphere

250:125999. https://doi.org/10.1016/j.chemosphere.2020.125999

Lin CY, Yu CJ, Lin YH, Tseng WL (2010) Colorimetric sensing of silver(I) and mercury (II) ions based on an assembly of tween 20-stabilized gold nanoparticles. Anal Chem. https://doi.org/10.1021/ac1007909

Lin H, Dai Q, Zheng L, Hong H, Wu F (2020) Radial basis function artificial neural network able to accurately predict disinfection by-product levels in tap water: taking haloacetic acids as a case study. Chemosphere 248:125999. https://doi.org/10.1016/j.chemosphere.2020.125999

Liu L, Zhang D, Zhang G, Xiang J, Zhu D (2008) Highly Selective Ratiometric Fluorescence Determination of Ag^+ Based on a Molecular Motif with One Pyrene and Two Adenine Moieties. Org Lett 10:2271–2274. https://doi.org/10.1021/ol8006716

Lotfia B, Aliakbar T, Peyman A, Maryam M, Ali A, Jacques M, Reza Z (2017) Multivalent calix[4]arene-based fluorescent sensor for detecting silver ions in aqueous media and physiological environment. Biosens Bioelectron 90:290–297. https://doi.org/10.1016/j.bios.2016.11.065

Lu H, Liang F, Gou J, Leng J, Du S (2014) Synergistic effect of Ag nanoparticle—decorated graphene oxide and carbon fiber on electrical actuation of polymeric shape memory nanocomposites. Smart Mater Struct 23:085034. https://doi.org/10.1088/0964-1726/23/8/085034

Luidmila S, Yakimova LH, Gilmanova VG, Evtugyn YN, Osin I, Stoikov I (2017) Self- assembled fractal hybrid dendrites from water-soluble anionic calix[4] werene and Ag^+. J Nanoparticle Res 19:173. https://doi.org/10.1007/s11051-017-3868-9

Lv Y, Zhu L, Liu H, Wu Y, Chen Z, Fu H, Tian Z (2014) Single-fluorophore- based fluorescent probes enable dual-channel detection of Ag^+ and Hg^{2+} with high selectivity and sensitivity. Anal Chim Acta 839:74–82. https://doi.org/10.1016/j.aca.2014.06.010

Mikelova R, Baloun J, Petrlova J, Adam V, Havel L, Petrek J, Horna A, Kizek R (2007) Electrochemical determination of Ag-ions in environment waters and their action on plant embryos. Bioelectrochemistry 70:508–518. https://doi.org/10.1016/j.bioelechem.2006.12.001

Nam T, Kyu J, Doo O, Singh N, Goh H (2017) Dipodal colorimetric sensor for Ag^+ and its resultant complex for iodide sensing using a cation displacement approach in water. Tetrahedron Lett 58:1040–1045. https://doi.org/10.1016/j.tetlet.2017.01.098

Nasrollahzadeh M, Sajjadi M, Iravani S, Varma RS (2020) Green synthesized nanocatalysts and nanomaterials for water treatment: current challenges and future perspectives. J Hazard Mater. https://doi.org/10.1016/j.jhazmat.2020.123401

Park JH, Kumar N, Park DH, Yusupov M, Neyts EC, Verlackt C, Bogaerts A, Kang MH, Uhm HS, Choi EH (2015) A comparative study for the inactivation of multidrug resistance bacteria using dielectric barrier discharge and nanosecond pulsed plasma. Sci Rep 5:13849. https://doi.org/10.1038/srep13849

Prasannan A, Imae T (2013) One-pot synthesis of fluorescent carbon dots from orange waste peels. Ind Eng Chem Res 52:15673–15678. https://doi.org/10.1016/j.matlet.2014.08.111

Rao L, Tang J, Hu S, Shen L, Lin H (2020) Inkjet printing assisted electroless Ni plating to fabricate nickel coated polypropylene membrane with improved performance. J Colloid Interface Sci 565:546–554. https://doi.org/10.1016/j.jcis.2020.01.069

Singha S, Kim D, Seo H, Cho SW, Ahn KH (2015) Fluorescence sensing systems for gold and silver species. Chem Soc Rev 44:4367–4399. https://doi.org/10.1039/c4cs00328d

Spokoyny AM, Dongwoo K, Abdelqader S, Mirkin CA (2009) Infinite coordin ation polymer nano-and microparticle structures. Chem Soc Rev 38:1218–1227. https://doi.org/10.1039/b807085g

Tabaraki R, Nateghi A (2016) Nitrogen-doped graphene quantum dots: "turn-off" fluorescent probe for detection of Ag^+ ions. J Fluoresc 26:297–305. https://doi.org/10.1007/s10895-015-1714-y

Teng X, Huang S, Jian W, Wang H, Qiao Z, Yong Y, Ma X (2018) Fabrication of Fe2C embedded in hollow carbon spheres: a high-performance and stable catalyst for fischer-tropsch synthesis[J]. ChemCatChem 10:3883–3891. https://doi.org/10.1002/cctc.201800488

Teng J, Shen L, Xu Y, Chen Y, Lin H (2020a) Effects of molecular weight distribution of soluble microbial products (SMPs) on membrane fouling in a membrane bioreactor (MBR): novel mechanistic insights. Chemosphere 248:126013. https://doi.org/10.1016/j.chemosphere.2020a.126013

Teng J, Wu M, Chen J, Lin H, He Y (2020b) Different fouling propensities of loosely and tightly bound extracellular polymeric substances (EPSs) and the related fouling mechanisms in a membrane bioreactor. Chemosphere 255:126953. https://doi.org/10.1016/j.chemosphere.2020b.126953

Vaishnav JK, Mukherjee TK (2019) Surfactant-induced self-assembly of CdTe quantum dots into multicolor luminescent hybrid vesicles. Langmuir. https://doi.org/10.1021/acs.langmuir.9b00357

Velmurugan K, Raman A, Easwaramoorthi S, Nandhakumar R (2014) Pyrene pyridine-conjugate as Ag selective fluorescent chemosensor. RSC Adv 4:35284–35289. https://doi.org/10.1039/c4ra04001e

Wang JH, Wang HQ, Zhang HL, Li XQ, Hua XF, Cao YC, Huang ZL, Zhao YD (2007) Purification of denatured bovine serum albumin coated CdTe quantum dots for sensitive detection of silver(I) ions. Anal Bioanal Chem 388:969–974. https://doi.org/10.1007/s00216-007-1277-0

Wang S, Bao X, Gao B, Li M (2019) A novel sulfur quantum dot for the detection of cobalt ions and norfloxacin as a fluorescent "switch". Dalton Trans 48:8288–8296. https://doi.org/10.1039/c9dt01186b

Wang S, Bao X, Gao B, Li M (2019) A novel sulfur quantum dot for the detection of cobalt ions and norfloxacin as a fluorescent "switch." Dalton Trans 48:8288–8296. https://doi.org/10.1039/c9dt01186b

Wu M, Chen Y, Lin H, Zhao L, Shen L, Li R, Xu Y, Hong H, He Y (2020) Membrane fouling caused by biological foams in a submerged membrane bioreactor:

mechanism insights [J]. Water Res 181(115932):https://doi.org/10.1016 /j.waters.115932

Xiao Y, Cui X, Zheng Q, Xiang S, Qian G, Chen J (2010) A microporous luminescent metal-organic framework for highly selective and sensitive sensing of Cu^{2+} in aqueous solution. Chem Commun Royal Soc Chem. 46:5503–5505. https://doi.org/10.1039/c0cc00148a

Yakimova LS, Gilmanova LH, Evtugyn VG, Osin YN, Stoikov II (2017) Self-assembled fractal hybrid dendrites from water-soluble anionic (thia)calix[4] arenes and Ag^{+}. J Nanopart Res 19:173. https://doi.org/10.1007/s11051-017-3868-9

Yang Y, Liu Y, Chen S, Cheong KL, Teng B (2020) Carboxymethyl β-cyclodextrin grafted carboxymethyl chitosan hydrogel-based microparticles for oral insulin delivery. Carbohyd Polym 246:116617. https://doi.org/10.1016/j.carbpol.2020.116617

Zhang Y, Ye A, Yao Y, Yao C (2019) A sensitive near-infrared fluorescent probe for detecting heavy metal Ag^{+} in water samples. Sensors 19:2471/1-3247. https://doi.org/10.3390/s19020247

Zhang C, Hu M, Ke Q, Guo C, Guo Y (2020) Nacre-inspired hydroxylapatite/chitosan layered composites effectively remove lead ions in continuous-flow wastewater. J Hazard Mater 386:121999. https://doi.org/10.1016/j.jhazmat.2019.121999

Zheng M, Xie Z, Li D, Du P, Jing X et al (2013) On-off-on fluorescent carbon dot nanosensor for recognition of chromium(VI) and ascorbic acid based on the inner filter effect. ACS Appl Mater Interfaces 5:13242–13247. https://doi.org/10.1021/am4042355

Zhou W, Li T, Yuan M (2021) Decoupling of inter-particle polarization and intra-particle polarization in core-shell structured nanocomposites towards improved dielectric performance. Energy Storage Mater 42:1–11. https://doi.org/10.1016/j.ensm.2021.07.014